Supplementary material

Smartphone-assisted detection of nucleic acids by light-harvesting FRET-based nanoprobe

Caterina Severi, Nina Melnychuk, and Andrey S. Klymchenko*

Laboratoire de Bioimagerie et Pathologies, UMR 7021 CNRS, Faculté de Pharmacie, Université de Strasbourg, France

*e-mail: andrey.klymchenko@unistra.fr

Table of Contents

1. Experimental section

1.1. Chemical compounds

Poly (methyl methacrylate-co-methacrylic acid) (PMMA-MA, 1.6% methacrylic acid, M_n ~15000, M_w ~34000), 3-chloropropylamine hydrochloride (98%), Rhodamine 6G (95.0%), Rhodamine 110 (>99.0%), 1-octadecanol (95%), 4-(Dimethylamino)pyridine (≥99%), N-(3-Dimethylaminopropyl)-N′-ethylcarbodiimide hydrochloride (≥98%), sodium tetrakis[3,5-bis(1,1,1,3,3,3-hexafluoro-2-methoxy-2-propyl)phenyl]borate trihydrate (Selectophore™), N,N-Diisopropylethylamine (≥99%), acetonitrile (anhydrous, 99.8%), dichloromethane (anhydrous, ≥99.8%), 1-Hydroxybenzotriazole (≥97%), 3- azido-1-propamine (≥95%), BSA-biotin, Amicon Centrifugal filters (0.5mL, 100K) were purchased from Sigma-Aldrich. Citric acid monohydrate (≥99.5%), sodium azide (99%), sodium iodide (≥99.5%) and trifluoroacetic acid (99%) were purchased from Alfa Aesar. FmocAsp(OtBu)-OH was purchased from Activotec. HBTU was purchased from ChemPep Inc. Neutravidin, LabTek chambers (Borosilicate cover glass, eight wells) and MultiSpeck™ Multispectral Fluorescence Microscopy Standards

Kit (M-7901) were purchased from ThermoFisher Scientific. Sodium phosphate monobasic (>99.0%, Sigma-Aldrich) and sodium phosphate dibasic dihydrate (>99.0%, Sigma- Aldrich) were used to prepare 20 mM phosphate buffers at pH 7.4. For saline buffer sodium chloride (≥99%, Sigma Aldrich) 30 mM and magnesium chloride (≥98%, Sigma Aldrich) 12 mM was added to 20 mM phosphate buffer and pH was adjusted with sodium hydroxide 1N solution. Milli-Q water (Millipore) was used in all experiments. For immobilization protocol PBS (without Ca^{2+} and Mg^{2+}) was purchased from Lonza.

1.1.1. Oligonucleotides

Single stranded lyophilized DNA sequences were purchased from IBA, then dissolved in MilliQ water and stored at -20 °C. The sequences used in this work are the following.

SurC-DBCO: 5′-CCC AGC CTT CCA GCT CCT TGA-(DBCO)-3′

T20-DBCO: 5′-TTT TTT TTT TTT TTT TTT TT-(DBCO)-3′

TCS-ATTO647N: 5′-(ATTO647N)- TCA AGG AGC TGG-3′

Target: 5′-CAA GGA GCT GGA AGG CTG GG-3′

A20-Biotin: 5′-(Biotin)-AAA AAA AAA AAA AAA AAA AA-3′

1.2. Protocols of synthesis

1.2.1. Synthesis of PMMA-AspN3

PMMA-AspN3 was synthesized following a previously described procedure (Melnychuk and Klymchenko, 2018).

1.2.2. Synthesis of F9-Al counterion

F9-Al counterion was synthesized following previously described procedures (Krossing, 2001; Andreiuk et al., 2017).

1.2.3. Synthesis of Rhodamine 110 octadecyl ester

Green-emitting dye Rhodamine 110 octadecyl ester (R110-C18) was synthesized according to a previously described procedure (Floyd et al., 2008).

Rhodamine 110 (80 mg, 0.21 mmol) and 1-octadecanol (2 g, 7.40 mmol) were mixed together and heated at 80 °C, when the octadecanol dissolved completely concentrated sulfuric acid (0.1 mL) was added. The system was stirred for 48 hours, then 0.6 mL of triethylamine were slowly added. Then the reaction was cooled down at room temperature and to the resulting red solid 200 mL of diethyl ether were added, the system stirred for one hour. The reaction mixture was filtrated and a red solid was obtained. Crude product was purified over preparative TLC using 9:1 DCM/MeOH as an eluent. 72 mg of R110-C18 were obtained (59% yield).

1.2.4. Synthesis of Rhodamine 6G octadecyl ester

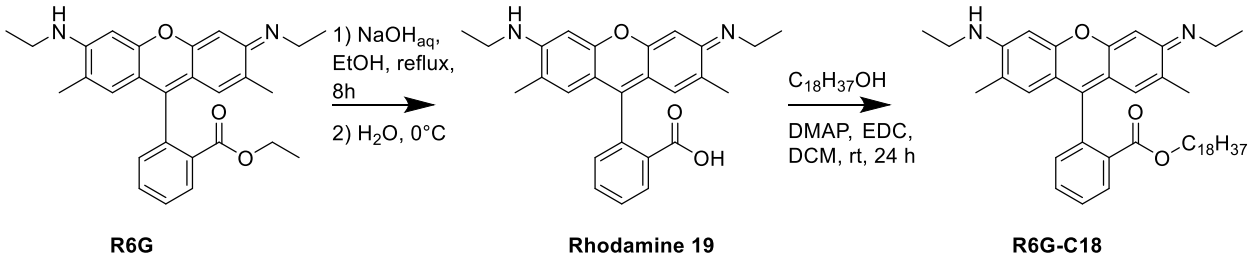

Scheme S1 *Synthesis of R6G-C18*

Rhodamine 19 was prepared according to an already described procedure (Yang et al., 2009).

To a solution of Rhodamine 6G (1 g, 2.1 mmol) in ethanol (20 mL) aqueous sodium hydroxide was added (250 mg, 6.3 mmol in 6 mL). System was refluxed for 8 hours, then the solution was allowed to cool at room temperature and distilled water (10 mL) was added. System was cooled at 0 °C and a red-purple solid started precipitating. The as-obtained precipitate was filtered and dried to obtain 563 mg (1.25 mmol, 59% yield) of Rhodamine 19.

To a solution of Rhodamine 19 (200 mg, 0.44 mmol), 1-octadecanol (360 mg, 1.33 mmol) and 1-Ethyl-3-(3-dimethylaminopropyl)carbodiimide hydrochloride (425 mg, 2.22 mmol) in dichloromethane (5 mL), DMAP (11 mg, 0.09 mmol) was added. Reaction was left stirring at room temperature under argon for 24 hours. Then the reaction was washed three times with HCl 1M and one time with brine. Organic fraction was gathered and solvent evaporated, finally the crude product was purified via silica chromatography using DCM/MeOH 95/5 as eluent. 230 mg of Rhodamine 6G octadecyl ester (R6G-C18) were obtained (78% yield). ^{1}H NMR (400 MHz, CD_3OD) δ ppm 0.91 (3 H, t, *J*=7.9 Hz) 1.03-1.36 (34H, m) 1.40 (6H, t, *J*=7.17 Hz) 2.16 (6H, s) 3.56 (4H, q, *J*=7.17) 3.93 (2H, t, *J*=6.16 Hz) 6.92 (2H, d, *J*=1.05 Hz) 6.97 (2H, s) 7.43 (1H, dd, *J*=7.31 Hz *J*=1.34 Hz) 7.82-7.91 (2H, m) 8.32 (1H, dd, *J*=7.61 Hz *J*=1.44). ^{13}C NMR (126 MHz, CD_3OD) δ ppm 169.58 (s) 161.92 (s) 161.50 (s) 160.28 (s) 137.28 (s) 136.51 (s) 134.90 (s) 134.81 (s) 134.56 (s) 134.12 (s) 134.00 (s) 132.63 (s) 129.50 (s) 117.36 (s) 97.42 (s) 69.24 (s) 42.02 (s) 35.61 (s) 33.31 (s) 33.29 (s) 33.28 (s) 33.24 (s) 33.05 (s) 33.01 (s) 32.81 (s) 31.92 (s) 29.49 (s) 26.27 (s) 20.14 (s) 16.98 (s) 16.63 (s). HRMS (m/z): $[M]^+$ calcd. for $C_{44}H_{63}N_2O_3$ 667.4839; found 667.4833.

1.2.5. Synthesis of dye salts

The salts of octadecyl rhodamine 110 and octadecyl rhodamine 6G with different counterions were prepared by ion exchange followed by purification over silica chromatography.

R110-C18/F9-Al. R110-C18/Cl (1 eq, 3 mg, 0.0048 mmol) and lithium tetrakis(perfluoro-tertbutoxy)aluminate (F9-Al) (3 eq, 14 mg, 0.015 mmol) were mixed in 1 mL of dichloromethane. TLC analysis showed instant conversion. The final product was then purified over silica column using DCM/MeOH 9/1 as eluent. Evaporation of solvent yielded 6 mg of product (corresponding to 81% yield). ^{1}H NMR (400 MHz, CD_3OD) δ ppm 0.88 (3 H, t, *J*=7.09 Hz) 1.05-1.36 (34H, m) 6.79-6.82 (4H, m) 7.05 (2H, d, *J*=9.28 Hz) 7.40 (1H, dd, *J*=7.26 Hz, *J*=1.36 Hz) 7.75-7.89 (2H, m) 8.28 (1H, dd, *J*=7.65 Hz

J=1.36). ^{19}F NMR (376 MHz, $CDCl_3$) δ ppm -76.15 (36 F, s). ^{27}Al NMR (130 MHz, CD_3OD) δ ppm 38.2 (1 Al, s). ^{13}C NMR (126 MHz, CD_3OD) δ ppm 212.63 (s) 169.46 (s) 163.92 (s) 163.88 (s) 162.23 (s) 137.11 (s) 136.45 (s) 135.48 (s) 134.46 (s) 134.04 (s) 123.10 (q, *J*=292.30 Hz) 120.52 (s) 117.48 (s) 100.97 (s) 69.37 (s) 35.59 (s) 33.29 (s) 33.27 (s) 33.24 (s) 33.22 (s) 33.19 (s) 33.03 (s) 32.99 (s) 23.84 (s) 31.94 (s) 29.55 (s) 26.25 (s) 16.94 (s) 3.28 (s). HRMS (m/z): $[M]^+$ calcd. for $C_{38}H_{51}N_2O_3$ 583.3900; found 583.3911; $[M]^-$ calcd. for $C_{16}AlF_{36}O_4$ 966.9037; found 966.9039.

R110-C18/F12. R110-C18/Cl (1 eq, 3 mg, 0.0048 mmol) and sodium tetrakis[3,5-bis(1,1,1,3,3,3-hexafluoro-2-methoxy-2- propyl)phenyl]borate trihydrate (F12) (3 eq, 28 mg, 0.015 mmol) were mixed in 1 mL of dichloromethane. TLC analysis showed instant conversion. The final product was then purified over silica column using DCM/MeOH 9/1 as eluent. Evaporation of solvent yielded 9 mg of product (corresponding to 82% yield). ^{1}H NMR (400 MHz, CD_3OD) δ ppm 0.86 (3 H, m) 1.12-1.41 (34H, m) 3.30 (24H, s), 6.85-6.60 (4H, m) 7.11 (2H, d, *J*=9.27 Hz), 7.42 (4H, bs) 7.47 (1H, dd, *J*=7.37 Hz, *J*=1.42 Hz), 7.58 (8H, bs), 7.83-7.92 (2H, m) 8.26 (1H, dd, *J*=7.63 Hz *J*=1.56). ^{19}F NMR (376 MHz, $CDCl_3$) δ ppm -71.29 (48 F, s). ^{11}B NMR (128 MHz, CD_3OD) δ ppm -5.95 (1 B, s). ^{13}C NMR (126 MHz, CD_3OD) δ ppm 212.62 (s) 169.45 (s) 163.92 (s) 163.88 (s) 162.23 (s) 161.39 (s) 137.84 (s) 137.11 (s) 136.45 (s) 135.47 (s) 134.45 (s) 134.03 (s) 126.51 (s) 123.61 (s) 122.23 (q, *J*=289 Hz) 120.52 (s) 117.48 (s) 100.97 (s) 69.36 (s) 35.58 (s) 33.28 (s) 33.27 (s) 33.24 (s) 33.22 (s) 33.18 (s) 33.03 (s) 32.99 (s) 23.84 (s) 31.93 (s) 29.54 (s) 26.24 (s) 16.94 (s) 3.27 (s). HRMS (m/z): $[M]^+$ calcd. for $C_{38}H_{51}N_2O_3$ 583.3900; found 583.3873; $[M]^-$ calcd. for $C_{56}H_{36}BF_{48}O_8$ 1759.1737; found 1759.1770.

R6G-C18/F9-Al. R6G-C18/Cl (1 eq, 3 mg, 0.0043 mmol) and lithium tetrakis(perfluoro-tertbutoxy)aluminate (F9-Al) (3 eq, 12 mg, 0.013 mmol) were mixed in 1 mL of dichloromethane. TLC analysis showed instant conversion. The final product was then purified over silica column using DCM/MeOH 95/5 as eluent. Evaporation of solvent yielded 5 mg of product (corresponding to 71% yield). ^{1}H NMR (400 MHz, CD_3OD) δ ppm 0.88 (3 H, t, *J*=6.76 Hz) 0.99-1.33 (34H, m) 1.37 (6H, t, *J*=7.24 Hz) 2.13 (6H, s) 3.53 (4H, q, *J*=7.24) 3.90 (2H, t, *J*=6.20 Hz) 6.89 (2H, s) 6.94 (2H, s) 7.40 (1H, d, *J*=7.01 Hz) 7.77-7.88 (2H, m) 8.30 (1H, dd, *J*=7.67 Hz *J*=1.22). ^{19}F NMR (376 MHz, $CDCl_3$) δ ppm -75.50 (36 F, s). ^{27}Al NMR (130 MHz, CD_3OD) δ ppm 34.0 (1 Al, s). ^{13}C NMR (126 MHz, CD_3OD) δ ppm 165.67 (s) 158.02 (s) 157.57 (s) 156.35 (s) 133.32 (s) 132.53 (s) 130.91 (s) 130.63 (s) 130.16 (s) 130.05 (s) 128.69 (s) 122.16 (q, *J*=293 Hz) 113.43 (s) 93.46 (s) 65.30 (s) 38.07 (s) 31.66 (s) 29.35 (s) 29.34 (s) 29.32 (s) 29.28 (s) 29.10 (s) 29.05 (s) 28.86 (s) 27.96 (s) 25.54 (s) 22.31 (s) 16.14 (s) 13.01 (s) 12.65 (s). HRMS (m/z): $[M]^+$ calcd. for $C_{44}H_{63}N_2O_3$ 667.4839; found 667.4828; $[M]^-$ calcd. for $C_{16}AlF_{36}O_4$ 966.9037; found 966.9062.

R6G-C18/F12. R6G -C18/Cl (1 eq, 3 mg, 0.0043 mmol) and sodium tetrakis[3,5-bis(1,1,1,3,3,3-hexafluoro-2-methoxy-2- propyl)phenyl]borate trihydrate (F12) (3 eq, 24 mg, 0.013 mmol) were mixed in 1 mL of dichloromethane. TLC analysis showed instant conversion. The final product was then purified over silica column using DCM/MeOH 95/5 as eluent. Evaporation of solvent yielded 9 mg of product (corresponding to 88% yield). ^{1}H NMR (400 MHz, CD_3OD) δ ppm 0.65 (3 H, t, *J*=6.84 Hz) 1.07-1.40 (34H, m) 1.43 (6H, t, *J*=7.20 Hz) 2.20 (6H, s) 3.30 (24H, s) 3.60 (4H, q, *J*=7.20) 3.96 (2H, t, *J*=6.20 Hz) 6.95 (2H, s) 7.00 (2H, s) 7.42 (4H, bs) 7.45 (1H, dd, *J*=7.45 Hz *J*=1.37 Hz) 7.58 (8H, bs) 7.84-7.94 (2H, m) 8.36 (1H, dd, *J*=7.60 Hz *J*=1.37). ^{19}F NMR (376 MHz, $CDCl_3$) δ ppm -71.35. (48 F, s). ^{11}B NMR (128 MHz, CD_3OD) δ ppm -5.95 (1 B, s). ^{13}C NMR (126 MHz, CD_3OD) δ ppm 165.67 (s) 162.59 (s) 161.39 (s) 158.02 (s) 157.58 (s) 156.36 (s) 136.93 (s) 133.32 (s) 132.54 (s) 130.92 (s) 130.64 (s) 130.16 (s) 130.05 (s) 128.70 (s) 125.56 (s) 125.20 (s) 122.70 (s) 122.54 (q, *J*=288.18 Hz) 113.43 (s) 93.46 (s) 83.29 (sept., *J*= 28.5 Hz) 65.30 (s) 52.84 (s) 38.07 (s) 31.66 (s) 29.36 (s) 29.33 (s) 29.29 (s) 29.10 (s) 29.05 (s) 28.87 (s) 27.97 (s) 25.54 (s) 22.32 (s) 16.15 (s) 13.01 (s) 12.66 (s). HRMS (m/z): $[M]^+$ calcd. for $C_{44}H_{63}N_2O_3$ 667.4839; found 667.4818; $[M]^-$ calcd. for $C_{56}H_{36}BF_{48}O_8$ 1759.1737; found 1759.1781.

1.3. Nanoparticle preparation and characterization

1.3.1. Nanoparticles preparation

PMMA-AspN3 and different amounts of dye were dissolved in acetonitrile at polymer concentration of 2 mg/mL. This stock solution was quickly diluted in a ten-fold excess of phosphate buffer (20 mM, pH = 7.4) under shaking. Afterwards the acetonitrile was gently evaporated under vacuum.

1.3.2. DNA nanoprobe preparation

SurC-DBCO (at concentrations ranging from 0.5 μM to 3 μM) and T20-DBCO (at concentrations ranging from 20 μM to 21.5 μM) were added to a freshly prepared nanoparticles solution. The mixture was kept for 20 h at 40 °C without any stirring and protected from light. The mixture was then allowed to cool at room temperature. Annealing with TCS-ATTO647N was performed by adding the flare (at the same concentration of SurC-DBCO) to the DNA-nanoparticle mixture, then heating to 70 °C for 3 minutes. The mixture was cooled down to room temperature again and kept in the dark for 1 h. Purification from unreacted DNA strands was performed by diluting the mixture with 20 mM phosphate buffer containing 12 mM $MgCl_2$ and 30 mM NaCl, then centrifuging using centrifuge filter (Amicon, 0.5 mL, 100 kDa) at 1000 G for 2 min. The ultra-filtration was repeated 5 times. The as-prepared DNA nanoprobes were then stored at 4 °C in the dark.

1.3.3. Nanoparticles characterization

Nanoparticle size was determined *via* DLS on a Zetasizer Nano ZSP (Malvern Instruments S.A.). For the analysis the mean value of the size distribution per volume was taken. For spectroscopic characterization all solvents used were of spectroscopic grade and MilliQ water was used. Absorption spectra were recorded on a Cary-4000 scan UV-visible spectrophotometer (Varian). Excitation and emission spectra were recorded on a Spectrofluorometer FS5 (Edinburgh Instruments). The fluorescence spectra were recorded setting the excitation wavelength at 470 nm for R110-C18 and 488 nm for R6G-C18. Moreover, fluorescence spectra were corrected both for lamp fluctuations and detector response. Fluorescence quantum yield of nanoparticles loaded with donor dye were calculated using Fluorescein for R110-C18 (QY = 0.91 in NaOH 0.1 M (Brouwer, 2011)) with an absorbance <0.1 at 470 nm, and Rhodamine 6G for R6G-C18 (QY = 0.94 in EtOH (Brouwer, 2011)) with absorbance <0.1 at 488 nm. FRET efficiency was expressed as the semi-quantitative FRET ratio:

$$E_{FRET} = \frac{A}{A + D}$$

Where D is the donor intensity at the maximum and A is the acceptor intensity. Antenna effect (AE), which represents the amplification factor of the acceptor emission was calculated as the ratio of the excitation intensity at the maximum of the donor and the excitation intensity at the maximum of the acceptor, correcting it by the emission of the donor dyes at 680 nm (Trofymchuk et al., 2017):

$$AE = \frac{I^{ex}_{D-FRET} - I^{ex}_{D} * \frac{I^{em}_{D-FRET}}{I^{em}_{D}}}{I^{ex}_{A-FRET} - I^{ex}_{A}}$$

Where I^{ex}_{D-FRET} and I^{ex}_{A-FRET} represent the excitation intensity of donor and acceptor at their respective maxima. I^{ex}_{D} and I^{ex}_{A} are the excitation intensities at the maximum wavelengths of donor and acceptor in the sample without acceptor. I^{em}_{D-FRET} and I^{em}_{D} are the maximum emission intensities of the donor in the samples with and without acceptor.

1.3.4. Estimation of number of dyes per nanoparticle

Using the diameter of the nanoparticles measured by DLS we calculated the volume of a nanoparticle assuming a spherical shape. Then, we calculated the approximate amount of dye molecules encapsulated in each nanoparticle of a given volume: the number of moles of the dye per unit of volume of a single particle is calculated from the dye loading inside the polymer matrix (250 mM), and multiplying this value by the Avogadro constant yields an approximate number of donor dye molecules per nanoparticle (~6000). We estimated the number of FRET acceptor molecules on the surface of the nanoparticles based on the absorption spectra of the DNA probes (Figure S7) by calculating the concentration of the acceptor and the donor at their respective absorption maxima, then the number of TCS-ATTO647N per NPs were estimated to be 6000 × c(acceptor)/c(donor).

1.3.5. Fluorescence microscopy

NPs were immobilized in LabTek following a previously described protocol (Schmied et al., 2014). The LabTek chamber was washed three times with PBS, then incubated with a solution of BSA-Biotin (0.5 mg/mL in PBS) for 10 min. Then the BSA-biotin solution was removed, and the chamber washed with PBS 3 times. The chamber then was incubated with a solution of neutravidin (0.5 mg/mL in PBS) for 10 minutes and washed again 3 times with PBS. Then, a solution of A20-biotin (1 µM in PBS) was added and left incubating for another 10 min, afterwards the chamber was washed 3 times with 20 mM phosphate buffer pH = 7.4 containing 12 mM $MgCl_2$ 30 mM and NaCl. Finally, the NPs solution at the appropriate concentration to obtain the desired density on the surface was incubated for 15 minutes in the dark. Chamber was then washed two more times with 20 mM phosphate buffer (pH = 7.4) containing

12 mM $MgCl_2$ and 30 mM NaCl, the same buffer for the measurements. Single-particle measurements were performed with a Nikon Ti-E inverted microscope with a 60x objective (Apo TIRF, oil, NA 1.49, Nikon) in the epifluorescence mode. Excitation source was a laser (Oxxius) at 488 nm and the power density was set at 2 $W \cdot cm^{-2}$ throughout all the experiments. For monochrome microscopy the fluorescence signal was recorded with Hamamatsu Orca Flash 4 camera and the exposure time was set to 200 ms per image frame. To enable a two-channel detection, corresponding to the donor and acceptor channel, W-VIEW GEMINI image splitting system (Hamamatsu) was used with dichroic 640 nm (Semrock FF640-FDi01-25x36). For RGB microscopy measurements the signal was recorded with a Nikon DS-Fi3 camera, the exposure time was set at 500 ms per image frame. For data acquired with both the monochrome camera and the RGB camera the ratiometric images were obtained by summing 10 image frames and then using an ImageJ plugin (developed by Roman Vauchelles, available upon request). The plugin divides the red channel image by the green channel image; for each pixel a pseudo-color scale is employed for coding the ratio, while the intensity corresponds to the integral intensity recorded for both channels at the corresponding image. For smartphone-based measurements an iPhone SE was used with an app (Halide developed by Ben Sandofsky) which allowed acquiring RAW images and controlling camera parameters. The images were recorded with a shutter exposure of 1/3 of a second and an ISO of 2000. Data analysis of the as-acquired images was performed as described above.

1.3.6. Detection of survivin oligonucleotide target

Detection in solution was performed by diluting the DNA probe in 20 mM phosphate buffer containing 30 mM NaCl and 12 mM $MgCl_2$ to a concentration of 10 pM (corresponding to TCS-ATTO647N) and an aliquot of survivin oligonucleotide target was added. The solution was then incubated in the dark at 25 °C for 6 h. Detection of the target on a glass surface was done by adding the target oligonucleotide to the LabTek chamber containing the immobilized DNA probes; the system was then kept in the dark at room temperature when the incubation time was 3 h.

1.3.7. Calculation of limit of detection (LOD) and limit of quantification (LOQ)

LOD and LOQ were calculated by performing a linear fit on all the data points shown in Figure 4B and then using the following equations ("Recommendations for the definition, estimation and use of the detection limit," 1987):

$$LOD = 3 \cdot \frac{\sigma_B}{S}, LOQ = 10 \cdot \frac{\sigma_B}{S}$$

Where σ_B is the standard error of the intercept of the linear regression (corresponding to the noise of the control sample without the target) and S is the slope of the linear regression (corresponding to the sensitivity of the method). The parameters of the linear regression of the data shown in Figure 4B are reported in Table S2.

1.3.8. Calculation of the detection area by smartphone camera

To calculate the area of detection with the smarphone camera a calibration experiment where the same field of fluorescent beads (MultiSpeck™, Thermo Fisher) absorbed on a surface was imaged with both a scientific grade sCMOS camera and the smartphone RGB camera (Figure S12). The two as-acquired images were then overlaid and it was found that the pixel dimension of the smartphone images was 0.526 µm/px. The size of the images analyzed for smartphone-based DNA detection experiments was of 200px × 200px, meaning that the area of detection is 105 µm × 105 µm.

2. Supporting figures and tables

2.1. DLS measurements

Table S1. Nanoparticle diameters measured via dynamic light scattering for each ion pair and loading.[a]

	diameter (nm)			
	dye/counterion pair			
loading (mM)	R110/F9-Al	R110-C18/F12	R6G-C18/F9-Al	R6G-C18/F12
5	44 ± 2	39 ± 5	45 ± 1	45 ± 1
120	42 ± 1	37 ± 2	48 ± 5	43 ± 5
250	39 ± 1	42 ± 1	43 ± 2	44 ± 1

[a] Errors are standard deviation (n = 3).

2.2. Fluorescence and absorption spectroscopy

2.2.1. Donor nanoparticles

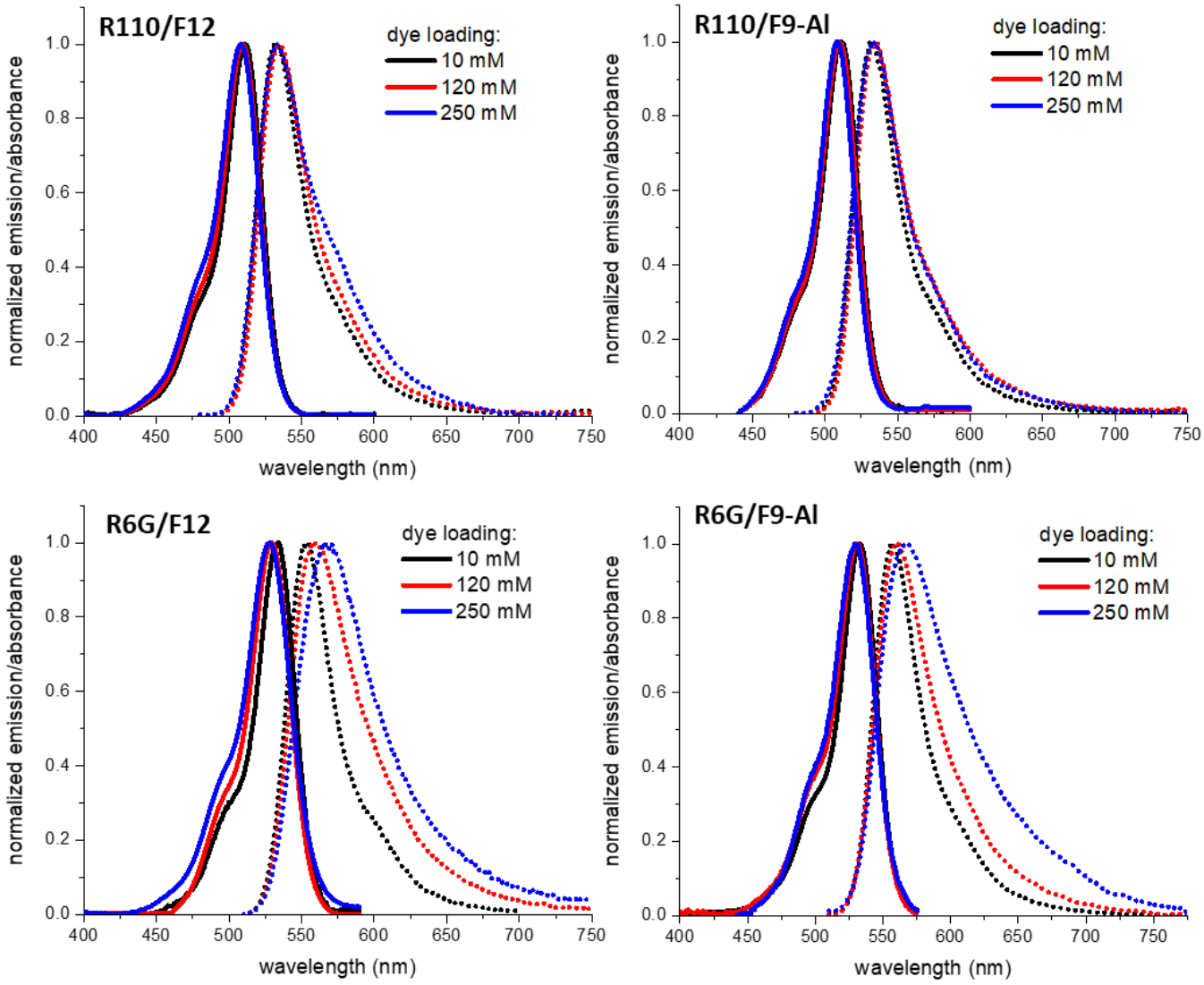

Figure S1. Normalized absorption and emission spectra of the polymeric NPs prepared with the four ion pairs at increasing dye loadings.

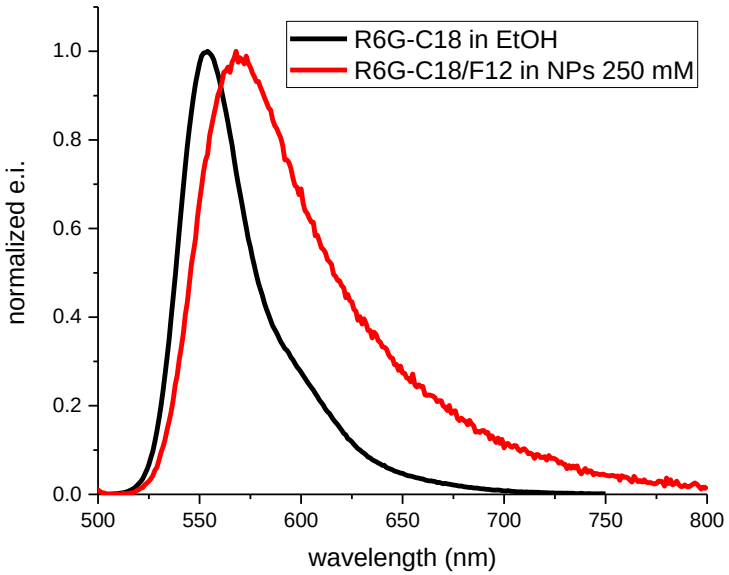

Figure S2. Emission of R6G-C18 in EtOH and in polymeric NPs loaded with R6G-C18 250 mM. A batochromic shift and an increase of the bandwidth due to partial aggregation of the dye inside the polymeric matrix is evident.

2.2.2. FRET studies with acceptor inside the NPs

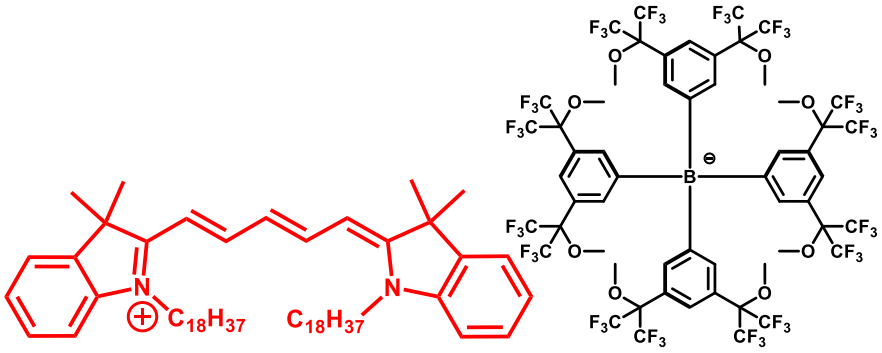

Figure S3. Structure of DID (with is counterion, F12), the FRET acceptor used in FRET studies with the acceptor inside the nanoparticles.

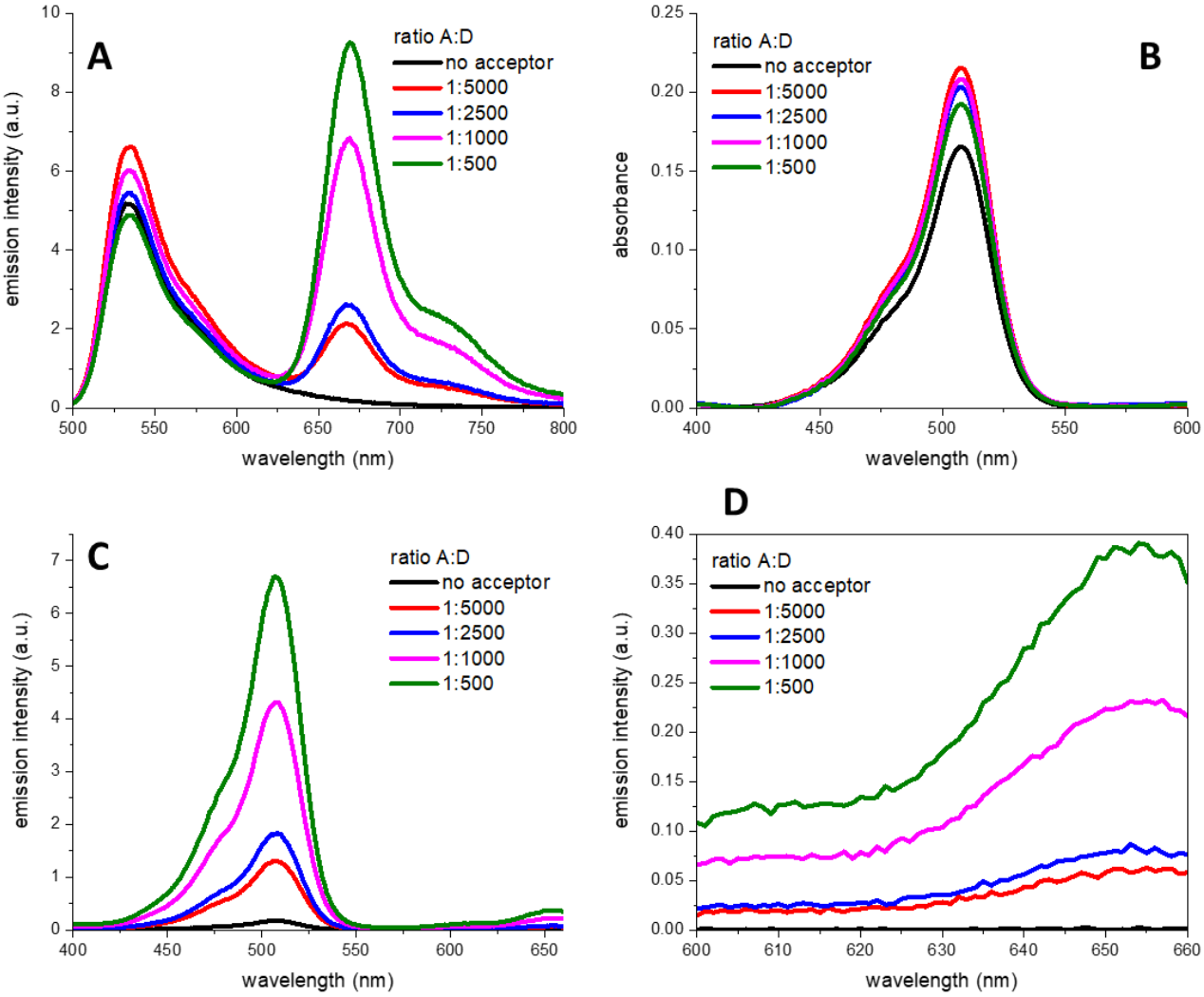

Figure S4. FRET studies: polymeric NPs encapsulating R110-C18/F9-Al at a 250 mM loading as a donor and a small quantity of DiD as an acceptor were prepared, and their FRET properties were tested, different acceptor/donor ratio were tested. (A) Emission spectra (λexc = 488 nm), (B) absorption spectra, (C) excitation spectra (λem = 670 nm), (D) zoom of the excitation spectra shown in (C).

R6G-C18/F12

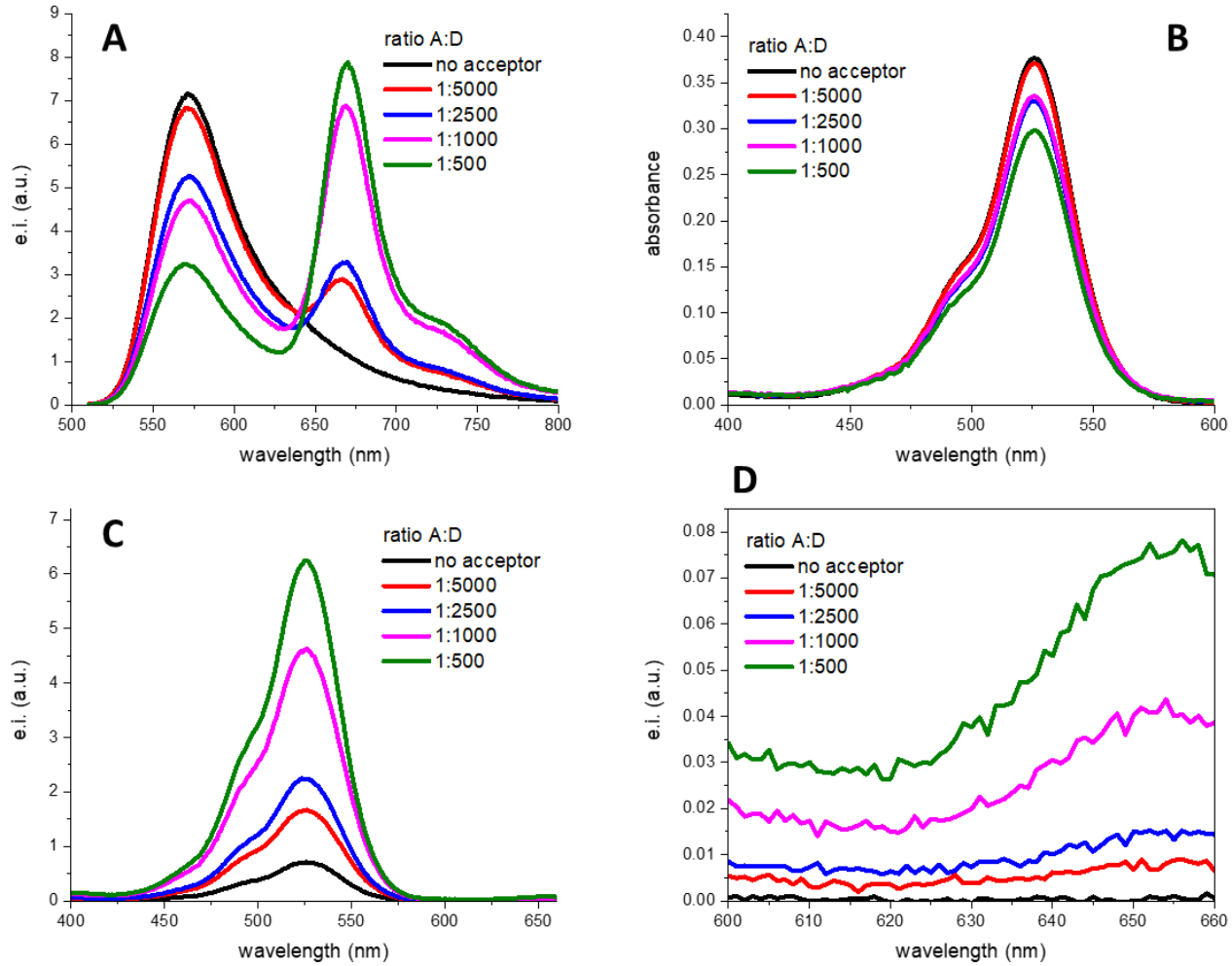

Figure S5. FRET studies: polymeric NPs encapsulating R6G-C18/F12 at a 250 mM loading as a donor and a small quantity of DiD as an acceptor were prepared, and their FRET properties were tested, different acceptor/donor ratio were tested. (A) Emission spectra (λexc = 488 nm), (B) absorption spectra, (C) excitation spectra (λem = 670 nm), (D) zoom of the excitation spectra shown in (C).

R6G-C18/F9-Al

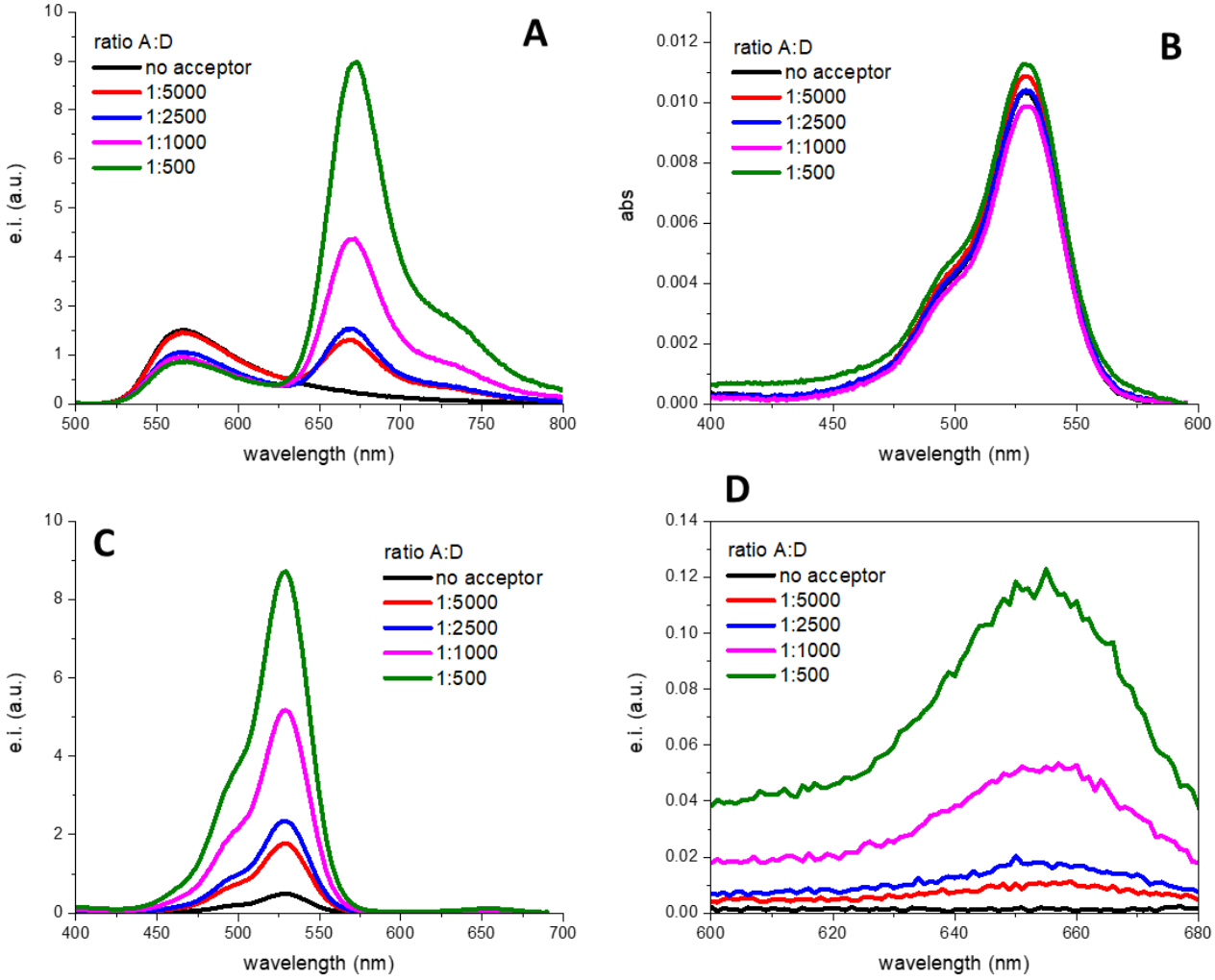

Figure S6. FRET studies: polymeric NPs encapsulating R110-C18/F9-Al at a 250 mM loading as a donor and a small quantity of DiD as an acceptor were prepared, and their FRET properties were tested, different acceptor/donor ratio were tested. (A) Emission spectra (λexc = 488 nm), (B) absorption spectra, (C) excitation spectra (λem = 690 nm), (D) zoom of the excitation spectra shown in (C).

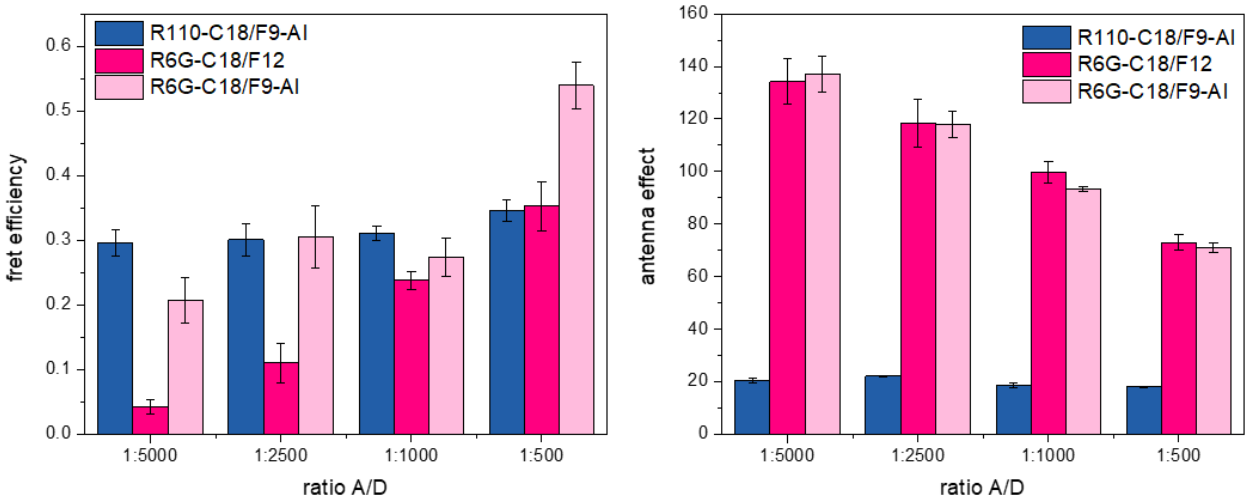

Figure S7. FRET efficiency (left) and antenna effect (right) of the three ion pairs as FRET donors inside NPs, previously shown as a function of acceptor to donor ratio based on the data in Figures S4-S6. Error bars are standard deviation (n = 3).

2.2.3. FRET studies with acceptor on the surface of the NPs

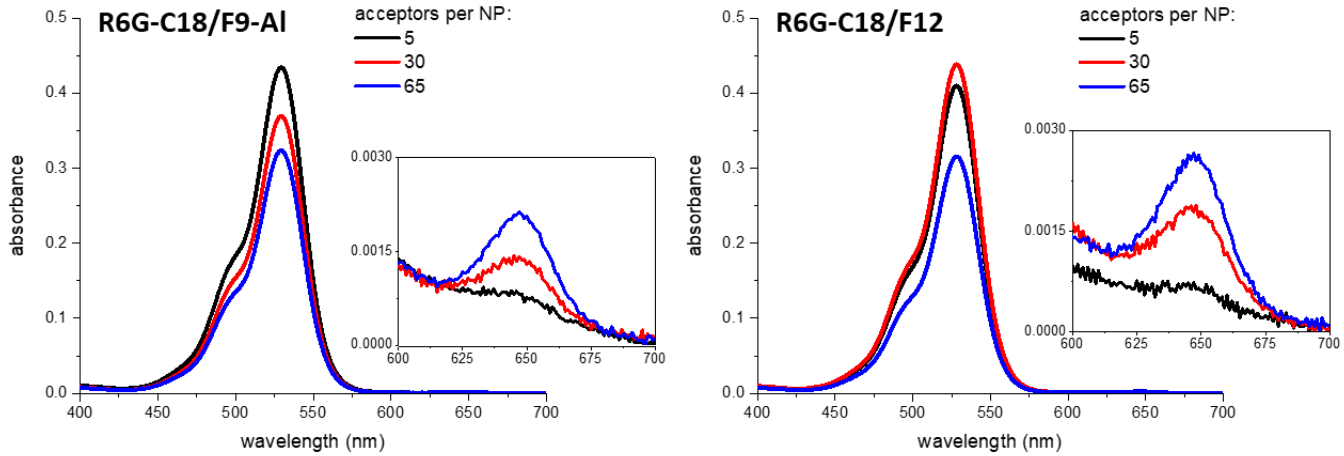

Figure S8. Absorption spectra of DNA-functionalized NPs encapsulating R6G-C18/F9-Al (left) and R6G-C18/F12 (right) with increasing quantities of acceptor (ATTO647N) at the surface, which allows calculation of the number of acceptors as described previously (Melnychuk and Klymchenko, 2018).

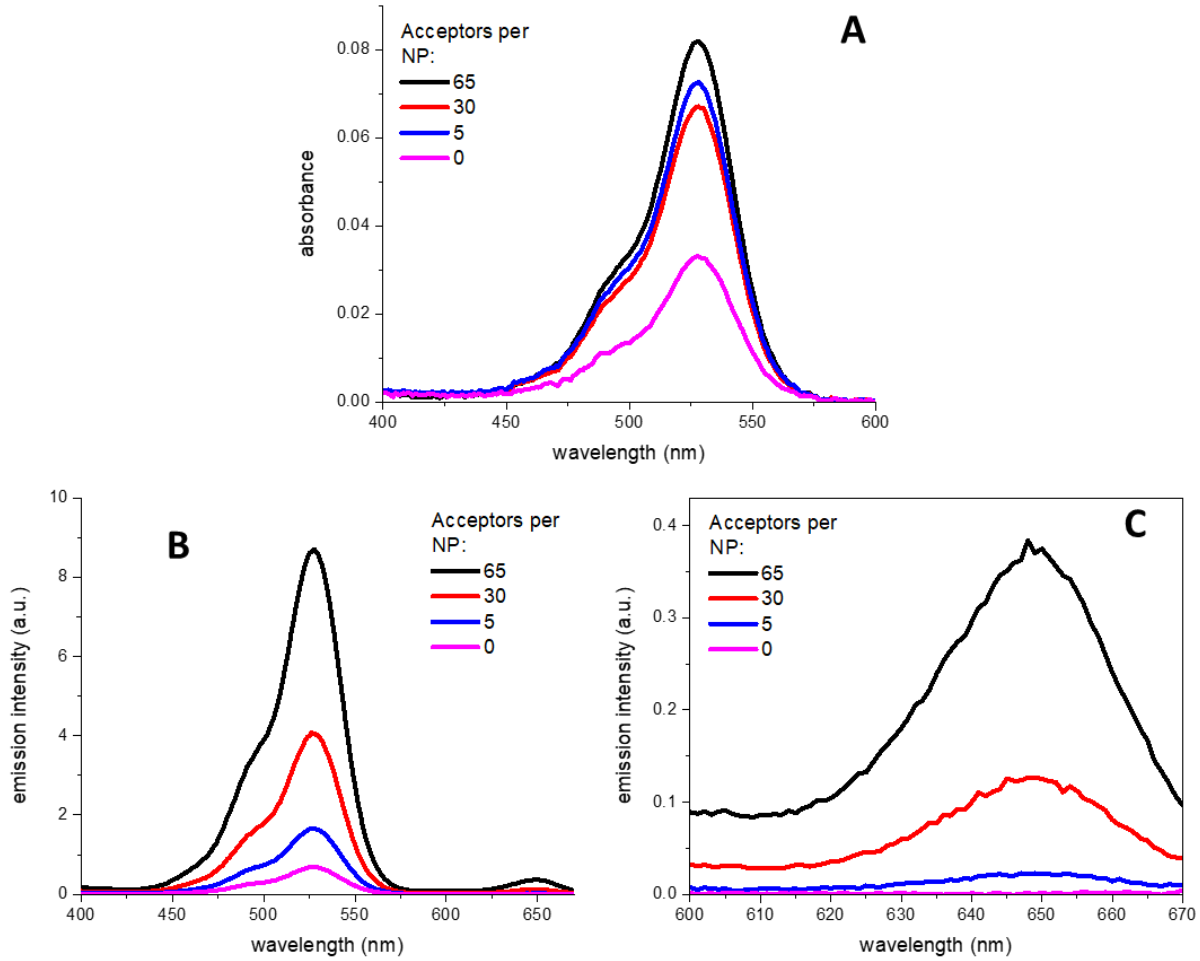

Figure S9. FRET studies on DNA-functionalized NPs encapsulating R6G-C18/F12 with a loading of 250 mM with the acceptor (ATTO647N) on the surface of the NPs with increasing quantity of acceptor. (A) absorption spectra, (B) excitation spectra (λem = 680 nm), (C) zoom on the acceptor part of the spectra shown in (C).

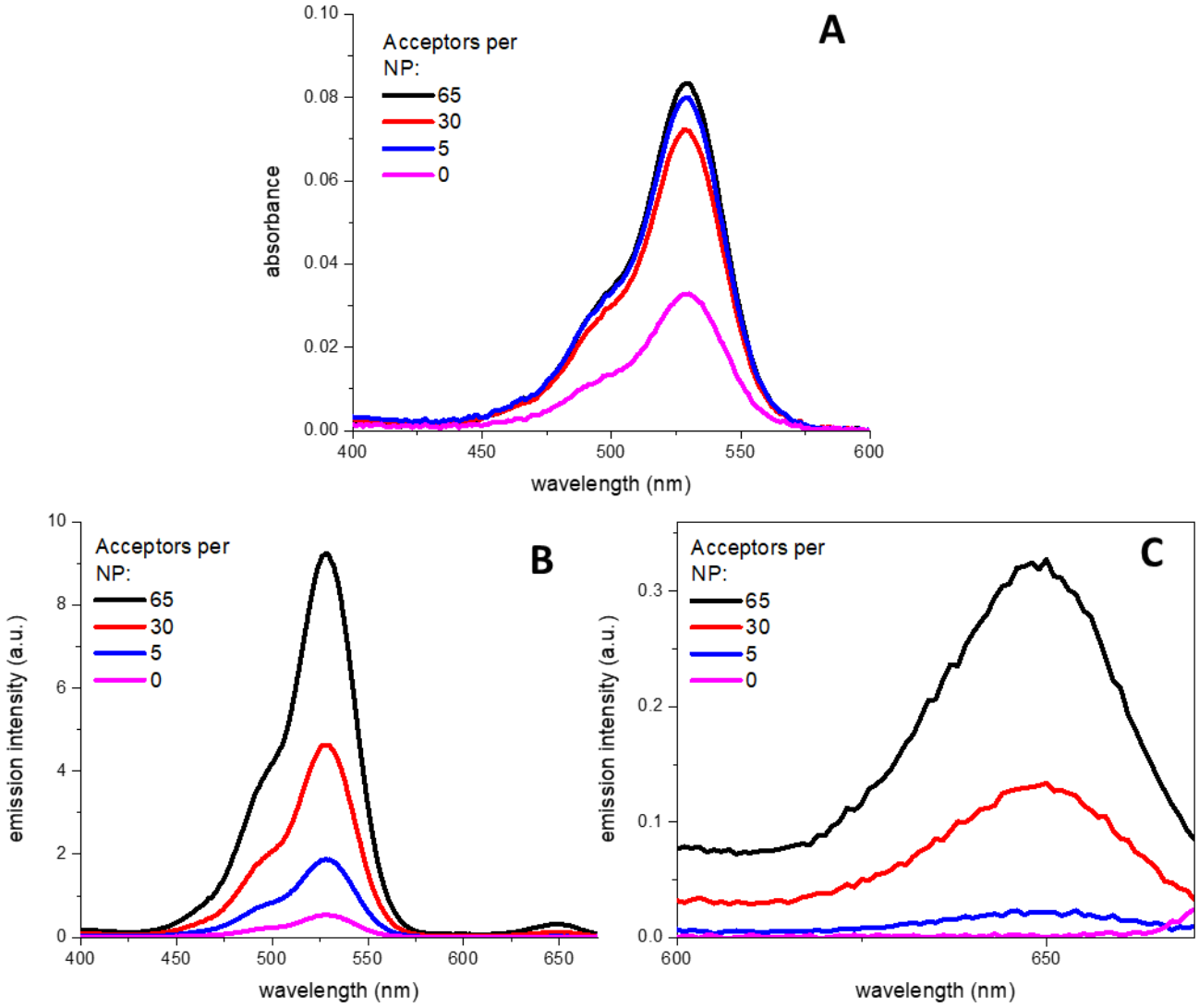

Figure S10. FRET studies on DNA-functionalized NPs encapsulating R6G-C18/F9-Al with a loading of 250 mM with the acceptor (ATTO647N) on the surface of the NPs with increasing quantity of acceptor. (A) absorption spectra, (B) excitation spectra (λem = 680 nm), (C) zoom on the acceptor part of the spectra shown in (C).

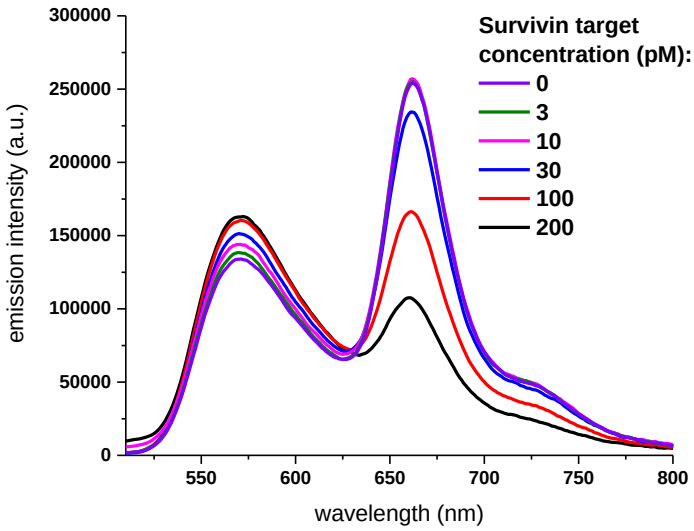

Figure S11. Non-normalized fluorescence spectra of NP-probe-65 incubated with increasing concentrations of the DNA target sequence. Data from Figure 4A.

Table S2 Parameters of the linear regression shown in Figure 3B,C.

Equation	y = a + b*x	
Residual Sum of Squares	28.0	
Pearson's r	-0.9971	
Adj. R-Square	0.9927	
	Value	Standard Error
Intercept	0.657	0.00115
Slope	-0.00135	5.17E-05

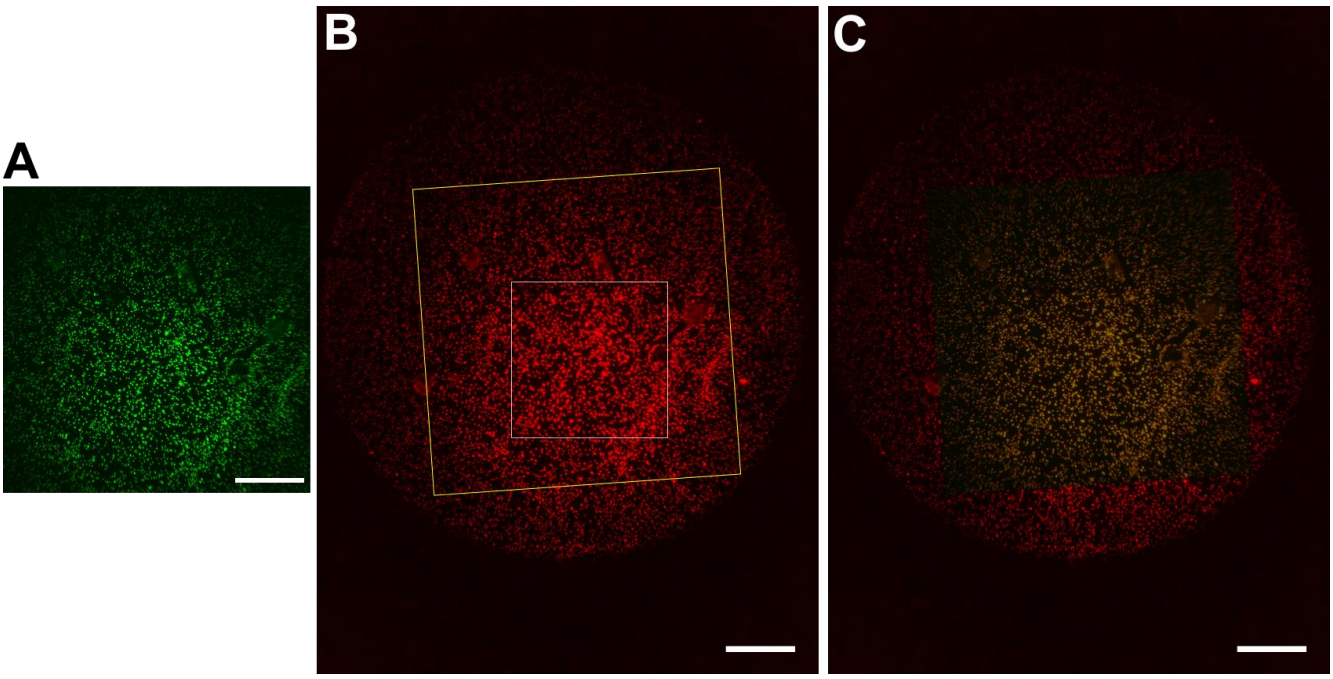

Figure S12. Estimation of the detection area of by the cellphone camera. (A) Microscopy image of fluorescent beads (MultiSpeck™, Thermo Fisher) acquired with sCMOS camera (Hamamatsu Orca Flash 4). (B) The same area of beads shown in (A) but acquired with the cellphone camera; yellow square represents the field captured in image (A), white square represents the area analyzed for DNA detection experiments. (C) Overlay between (A) and (B). Scale bars: 50 µm.

3. References

Andreiuk, B., Reisch, A., Pivovarenko, V.G., Klymchenko, A.S., 2017. Mater. Chem. Front. 1, 2309–2316.

Brouwer, A.M., 2011. Pure Appl. Chem. 83, 2213–2228.

Floyd, D.L., Ragains, J.R., Skehel, J.J., Harrison, S.C., van Oijen, A.M., 2008. Proc. Natl. Acad. Sci. 105, 15382–15387.

Krossing, I., 2001, Chem. – Eur. J., 7, 490–502.

Melnychuk, N., Klymchenko, A.S., 2018. J. Am. Chem. Soc. 140, 10856–10865.

Schmied, J.J., Raab, M., Forthmann, C., Pibiri, E., Wünsch, B., Dammeyer, T., Tinnefeld, P., 2014. Nat. Protoc. 9, 1367–1391.

Trofymchuk, K., Reisch, A., Didier, P., Fras, F., Gilliot, P., Mely, Y., Klymchenko, A.S., 2017. Nat. Photonics 11, 657–663.

Yang, Y.-K., Cho, H.J., Lee, J., Shin, I., Tae, J., 2009. Org. Lett. 11, 859–861.

1987. The Analyst 112, 199.